Earth Surface Processes and Landforms
Earth Surf. Process. Landforms (in press)
Published online in Wiley InterScience
(www.interscience.wiley.com) **DOI:** 10.1002/esp.1443

Coupling chemical weathering with soil production across soil-mantled landscapes

Benjamin C. Burke,[1,†] Arjun M. Heimsath[1]* and Arthur F. White[2]
[1] *Department of Earth Sciences, 6105 Fairchild Hall, Dartmouth College, Hanover, NH 03755, USA*
[2] *Water Resources Division, US Geological Survey, Menlo Park, CA 94025, USA*
[†] *Now at Exxon Mobil Exploration Co., 233 Benmar, Houston, TX77060, USA*

*Correspondence to: A. M. Heimsath, Department of Earth Sciences, 6105 Fairchild Hall, Dartmouth College, Hanover, NH 03755, USA.
E-mail: arjun.heimsath@clartmouth.edu

Received 4 January 2006;
Revised 27 July 2006;
Accepted 3 August 2006

Abstract

Soil-covered upland landscapes constitute a critical part of the habitable world. Our understanding of how they evolve as a function of different climatic, tectonic and geological regimes is important across a wide range of disciplines and depends, in part, on understanding the links between chemical and physical weathering processes. Extensive previous work has shown that soil production rates decrease with increasing soil column thickness, but chemical weathering rates were not measured. Here we examine a granitic, soil-mantled hillslope at Point Reyes, California, where soil production rates were determined using *in situ* produced cosmogenic nuclides (^{10}Be and ^{26}Al), and we quantify the extent as well as the rates of chemical weathering of the saprolite from beneath soil from across the landscape. We collected saprolite samples from the base of soil pits and analysed them for abrasion pH as well as for major and trace elements by X-ray fluorescence spectroscopy, and for clay mineralogy by X-ray diffraction spectroscopy. Our results show for the first time that chemical weathering rates decrease with increasing soil thickness and account for 13 to 51 per cent of total denudation. We also show that spatial variation in chemical weathering appears to be topographically controlled: weathering rate decreases with slope across the divergent ridge and increases with upslope contributing area in the convergent swale. Furthermore, to determine the best measure for the extent of saprolite weathering, we compared four different chemical weathering indices – the Vogt ratio, the chemical index of alteration (CIA), Parker's index, and the silicon–aluminium ratio – with saprolite pH. Measurements of the CIA were the most closely correlated with saprolite pH, showing that weathering intensity decreases linearly with an increase in saprolite pH from 4·7 to almost 7. Data presented here are among the first to couple directly rates of soil production and chemical weathering with how topography is likely to control weathering at a hillslope scale.

Keywords: saprolite; pH; landscape evolution; weathering indices; erosion

Introduction

Hillslope forms evolve over time as a result of total weathering, the sum of physical and chemical processes (e.g. Riebe *et al*., 2001, 2003a; Anderson *et al*., 2002; Stallard and Edmond, 1983). Total weathering is equivalent to erosion, the net removal of soil and other material from the hillslope, and results in landscape lowering in the absence of uplift. We consider physical weathering to be the mechanical processes that produce soil, defined here as the mobile layer of sediment being transported downslope. Chemical weathering – the dissolution and precipitation of minerals via subsurface flow – occurs along mineral grain boundaries and on mineral grains (White *et al*., 1999, 2001; Banfield and Eggleton, 1989), and results in a reduction of the coherence and potential strength of the bedrock (Kim and Park, 2003). The chemical weathering of the bedrock underlying a mobile soil mantle is thus critical to the soil production process (White *et al*., 1996; Paton *et al*., 1995; Mudd and Furbish, 2004) but has previously remained poorly quantified across soil-mantled landscapes.

We focus here on landscapes where the mass balance of the mobile soil column depends on soil production and erosion. Such landscapes have been studied widely and can be qualitatively characterized as either weathering- or

transport-limited (Carson and Kirkby, 1972). When erosion exceeds soil production, bedrock is exposed and erosion is weathering-limited. Conversely, when soil production is greater than erosion, soils will thicken creating a transport-limited landscape. When soil production equals erosion, a dynamic balance is reached such that soil depths are in a local steady state (Carson and Kirkby, 1972, Dietrich *et al*., 1995, Heimsath *et al*., 1997). Previous work showed that soil production rates decline with increasing overlying soil depth (e.g. Heimsath *et al*., 1997, 2000), such that there is a negative feedback between erosion and soil production, maintaining steady-state local soil depths. This work also showed that while soil thicknesses can be in a local steady state, they vary across the landscape such that soil production rates (and therefore denudation rates) are not constant at a landscape scale. The contribution of chemical weathering to the soil production process, both by helping to set the competence of the parent material as well as by removal of mass, remains poorly understood.

This paper addresses two aspects of hillslope evolution. First, we examine the quantitative relationship between chemical weathering and physical weathering. Heimsath *et al*. (1997) first established the method of using cosmogenic nuclide measurements to quantify soil production rates on soil-mantled hillslopes, determining that soil production rates decline exponentially with increasing soil depths. Heimsath *et al*. (2005) quantified a similar relationship at Point Reyes, California, but did not account for the chemical weathering of the saprolite. Addressing the determination of chemical weathering rates and building on the work of Brimhall *et al*. (1991, 1992), Riebe *et al*. (2001, 2003a, b) validated the use of a geochemical mass balance model to determine catchment-scale chemical weathering rates by coupling detrital zirconium concentrations with cosmogenic nuclide-derived total denudation rates. At a hillslope scale, Anderson *et al*. (2002) used extensive measurements of solute chemistry from an intensively studied catchment in the Oregon Coast Range and suggested that chemical denudation rates are secondary to physical weathering processes. These studies quantified critical connections between physical and chemical processes, but did not examine how chemical weathering is tied to sediment production processes. Here we couple directly physical soil production rates with chemical weathering at a hillslope scale.

Our second goal in this study is to use the morphometry of the landscape to suggest why differences in chemical weathering might occur across the landscape. Heimsath *et al*. (1997) assumed that sediment transport flux was linearly proportional to slope and found that hillslope curvature was a reasonable proxy for soil production, which is equivalent to landscape lowering with local steady-state conditions. Simply put, the more convex the hillslope, the thinner the soil depths and the higher the soil production rate. Recent work spatially integrated soil production rates to estimate sediment transport flux and suggested that the flux is proportional to the product of soil depth and slope (Heimsath *et al*., 2005), but also showed that the relationship between curvature and soil production rates remains the same. At the same field site used by Heimsath *et al*. (2000) in Australia, Green *et al*. (2006) used a conservative element mass-balance approach for saprolite and soil samples to show that chemical weathering intensity increases with distance from the watershed divide. We use a similar approach, coupled with previously determined soil production rates (Heimsath *et al*., 2005), to examine how the extent and rates of chemical weathering vary across our site and are correlated with topographic position.

Combined with determining chemical weathering intensity (i.e. a measure of the extent of weathering) in hillslope saprolite, we also examine the efficacy of several indices used to determine chemical weathering intensity. Four commonly used indices are applied here: the silicon–aluminium ratio (Ruxton, 1968), Parker's index of silicate weathering (Parker, 1970), the chemical index of alteration (Kirkwood and Nesbitt, 1991), and the Vogt ratio (Vogt, 1927). These indices quantify chemical weathering intensity by comparing changes in major and trace metal concentrations as ratios of mobile to immobile elements. We also use saprolite abrasion pH and clay mineralogy of the saprolite as measures of absolute weathering intensity and compare our pH-based findings to the most effective chemical weathering intensity index. While these indices do not quantify chemical weathering rates, they provide a measure of the weathered state of the saprolite underlying the mobile soil column. This weathered condition is likely to play a critical role in governing how physical processes disrupt the saprolite, and is therefore an important parameter in determining resistance to erosion.

Coupling Chemical and Physical Weathering

To examine the connections between chemical and physical weathering, we need to consider the physical parameters that underlie the theory and quantification of hillslope evolution. For a typical soil-mantled landscape, where sediment transport flux can be assumed to be a linear function of slope, Heimsath *et al*. (1997) showed that the soil production rate decreased exponentially with increasing soil column thickness. This quantified a theoretical framework developed by several previous studies (e.g. Ahnert, 1987; Anderson and Humphrey, 1989; Dietrich *et al*., 1995), and helped define the relationship equating total denudation, D, soil production rates, P_{soil}, and topographic curvature, the second derivative of elevation, z:

DOI: 10.1002/esp

Chemical weathering and soil production

$$D = P_{soil} = \varepsilon_0 e^{-\alpha H} = -K\nabla^2 z, \quad (1)$$

where ε_0 is the soil production rate at zero soil depth, $H = 0$, and K is analogous to a diffusion coefficient with units $L^2 T^{-1}$. The field data supporting this relationship are from cosmogenic nuclide analysis (^{10}Be and ^{26}Al) of saprolite and bedrock samples at the soil–bedrock interface from several different sites (Heimsath *et al*., 1997, 2000, 2005). Heimsath *et al*. (2005) built on this analysis to suggest that transport flux is likely to be proportional to the depth–slope product, rather than slope alone, but also showed exceptionally strong support for Equation 1 from the field site used here. Field observations and high-resolution GPS surveys enable measurements of curvature across the hillslope to connect hillslope form to weathering. To fully quantify the linkages between soil production and chemical weathering, we measure additional hillslope morphometric parameters such as slope, contributing surface area, and distance from the divide across a landscape where the soil production function is known.

Chemical Weathering Rate

We use a geochemical mass balance method to calculate bulk chemical weathering rates (CWRs) as described by Riebe *et al*. (2001, 2003a, b), and similar to that of Brimhall *et al*. (1991, 1992) and Anderson *et al*. (2002). Heimsath *et al*. (1997) showed that the soil production rate (P_{soil}), determined by *in situ* produced cosmogenic nuclide concentrations measured in saprolite samples is equal to the landscape denudation rate (D). The landscape denudation rate is equal to the sum of the chemical weathering rate (W) and the physical erosion rate (E), such that:

$$P_{soil} = D = E + W, \quad (2)$$

When $W = 0$, $D = E$, and soil production is balanced solely by physical erosion. When W is non-zero, the chemical weathering rate is simply:

$$W = D - E. \quad (3)$$

By focusing on conservative elements, such as zirconium (Zr), that are not mobile in solution, we can consider $W = 0$ and restate E as a fraction of D by considering that the product of the unweathered rock [Zr] equals the product of the saprolite [Zr] and the physical erosion rate:

$$[Zr]_{rock} \times D = [Zr]_{saprolite} \times E. \quad (4)$$

By substituting Equation 4 into Equation 2, the chemical weathering rate is determined as a function of denudation:

$$W = D\left(1 - \frac{[Zr]_{rock}}{[Zr]_{saprolite}}\right), \quad (5)$$

where D has units of m Ma^{-1} and is typically determined by cosmogenic nuclide analyses. Concentrations of zirconium are measured in mg kg^{-1}. For saprolite in an upland, soil-mantled, eroding landscape, the chemical weathering rate has been shown to be a fraction of the total denudation rate using this approach (Riebe *et al*., 2001, 2003a, b). An important mass-balance assumption enables this methodology to be applicable to determining saprolite chemical weathering rates across soil-mantled landscapes: namely, that for a given soil–saprolite profile, the soil production rate is equivalent to the total denudation rate (i.e. landscape lowering rate), which is valid as long as local soil thickness is in temporal steady-state (Heimsath *et al*., 1997). This assumption is empirically supported at a soil-mantled field site in southeastern Australia (Heimsath *et al*., 2000) with similar morphology to the field site used here (Heimsath *et al*., 2005). This empirical support tested extensive modelling efforts (Dietrich *et al*., 1995; Fernandes and Dietrich, 1997; Heimsath *et al*., 1999) from a nearby northern California field area that suggested that a local steady-state soil depth was an appropriate assumption. We apply the approach of using Zr concentrations in saprolite (rather than soils) specifically to quantify chemical weathering rates of the saprolite directly beneath the soil mantle where cosmogenic nuclide analyses have determined the rates of saprolite conversion to soil. We also apply measurements of different indices to quantify the weathered condition of the saprolite.

DOI: 10.1002/esp

Absolute Measurements of Weathering Intensity

Abrasion pH

As parent minerals, such as feldspars and biotite, react with acidic groundwater to create kaolinite and biotite–vermiculite, the pH of the saprolite decreases. Saprolites and soils become more acidic over time in temperate climates as hydrolysis and solution reactions increase the number of hydrogen ions adhering to mineral boundaries and clay mineral interlayers. The reaction sequence of saprolite acidification (McBride, 1994) can be represented, for example, as:

$$CO_2 + H_2O = H_2CO_3 \tag{6}$$

$$H_2CO_2 + 0{\cdot}5Ca^{2+} - \text{clay} = 0{\cdot}5Ca(HCO_3)_2 + H^+ - \text{clay}. \tag{7}$$

Unweathered granitic rocks have an abrasion pH near 7. Grant (1969) found that the abrasion pH of a slurry of ground-up saprolite and distilled water decreased as weathering intensity increased: a plot of abrasion pH against percentage of clay minerals showed the usefulness of this technique. Because of the strong correlation between the percentage of clay minerals and abrasion pH, we use this method as an absolute measure of chemical weathering intensity in saprolite to compare against measures of hillslope morphometry and chemical weathering rates.

Clay minerals

As primary minerals chemically weather, subsurface waters transport solutes and precipitate secondary minerals, usually in the form of clays. For example, the weathering of feldspar minerals provides Ca and Na for kaolinite (Moore and Reynolds, 1997; White *et al*., 1998; Murphy *et al*., 1998). Biotite weathering creates biotite–vermiculite (Banfield and Eggleton, 1988; Jeong and Kim, 2003; Schroeder *et al*., in press).

In granite, plagioclase feldspar has the highest dissolution rate both in laboratory experiments and in the field (White *et al*., 2001). Quantifying plagioclase feldspar and clay mineral occurrence in saprolite can therefore determine the relative intensity of chemical weathering. When a sample contains feldspathic minerals, such as albite and anorthite, the sample has a lower relative intensity of chemical weathering. Samples that contain only major secondary clay minerals such as biotite–vermiculite have higher intensities of chemical weathering. This approach to examining chemical weathering intensity is dependent on the heterogeneity of mineral availability within the parent material.

Chemical Weathering Indices

In comparison to the absolute measures of weathering intensity, we examine the efficacy of several chemical weathering indices: the Vogt ratio (Vogt, 1927; Kim and Park, 2003), the chemical index of alteration (Kirkwood and Nesbitt, 1991), Parker's index (Parker, 1970), and the silicon–aluminium ratio (Ruxton, 1968). These indices use major and trace element chemistry and various assumptions about weathering profile evolution and parent material composition to show changes in chemical weathering intensity. We test the efficacy of each of these indices because of the relatively mixed success of applying such indices by previous studies. In doing so we also emphasize that these comparisons of indices are to ensure redundancy in our methodology and not to duplicate the discussion of Duzgoren-Ayden *et al*. (2002), who provide a thorough review of using these indices to quantify the weathered condition of granite.

Vogt Ratio (VR)

This ratio, defined as

$$VR = \frac{Al_2O_3 + K_2O}{MgO + CaO + Na_2O}, \tag{8}$$

measures two conservative major element oxide concentrations against three labile element oxide concentrations (Vogt, 1927; Kim and Park, 2003). It is essentially a ratio of immobile to mobile major elements except that the numerator contains oxides of both a mobile and an immobile element. Increasing VR values indicate an increasing intensity of weathering. Vogt (1927) and Roaldset (1972) used this index on clays from Norwegian granites. Kim and

DOI: 10.1002/esp

Park (2003) found poor correlation between this index and a petrographically determined weathering grade in Korean granites.

Chemical index of alteration (CIA)

The degree of chemical weathering for granitic soils and saprolites can be quantified by applying the CIA (Kirkwood and Nesbitt, 1991), where all oxide concentrations are measured in weight percentages:

$$\mathrm{CIA} = \frac{\mathrm{Al_2O_3}}{\mathrm{Al_2O_3} + \mathrm{Na_2O} + \mathrm{K_2O} + \mathrm{CaO}}. \tag{9}$$

This index measures the proportion of a conservative, but not immobile, oxide to the sum of most major oxides found in granitic bedrock. While the CIA value for unweathered granite is unique depending on the particular granite in question, the average unweathered granite has a CIA of 60. Conversely, a highly weathered soil or saprolite has a CIA of between 90 and 100 (Kirkwood and Nesbitt, 1991; Nesbitt and Young, 1982).

Parker's index (PI)

Using concentrations of mobile elements, Parker's index divides each of four major elemental oxide concentrations by a value to normalize for bond strength and individual mobility. The index is defined by Parker (1970) as:

$$\mathrm{PI} = \left(\frac{2 \times \mathrm{Na_2O}}{0{\cdot}35}\right) + \left(\frac{\mathrm{MgO}}{0{\cdot}90}\right) + \left(\frac{2 \times \mathrm{K_2O}}{0{\cdot}25}\right) + \left(\frac{\mathrm{CaO}}{0{\cdot}70}\right). \tag{10}$$

The important assumption for this index is that hydrolysis of primary minerals is the main agent of silicate weathering. Decreasing PI values indicate an increasing intensity of weathering.

Silicon–aluminium ratio (SA)

The SA is a molecular ratio of a mobile to an immobile elemental oxide and is defined as:

$$\mathrm{SA} = \frac{\mathrm{SiO_2}}{\mathrm{Al_2O_3}}, \tag{11}$$

where the silica is assumed to form the mobile oxide and the aluminium is assumed to form the immobile oxide. A decreasing SA value indicates an increasing intensity of weathering. Ruxton (1968) notes that the silica loss must be related to the total elemental loss. Ruxton (1968) and Irfan (1996, 1999) found the SA index to be a good indicator of chemical weathering in granitic rocks and in well-drained, acid and humid environments where the end products are kaolin group minerals. Parker (1970) notes that silica mobility within most weathering profiles is irregular and total loss is usually small.

Sampling and Analytical Methods

To test the coupling between physical and chemical weathering, we collected samples of saprolite from the base of the soil–saprolite interface in soil pits dug across a soil-mantled landscape where soil production rates are known. Three separate samples of saprolite were collected from each location for bulk density analysis using a direct-push corer. We also collected depth profiles of saprolite samples from six manual borings across the hillslope. The borings were augured as deeply as possible, ideally to unweathered granite parent material. Saprolite samples from each of the pits were analysed using a Phillips model PW2400 X-ray fluorescence spectrometer (XRF) for labile oxides (SiO_2, Na_2O, CaO, Al_2O_3 and K_2O) and trace elements (Zr, Ce, Ti, U, Th, Y, Ni, Nb and Sr). For XRF preparation, 20 g of each sample was dried at 110 °C for 24 h. Each sample was powdered in a tungsten carbide grinding mill for 3 min and ashed at 920 °C for 12 hours in a muffle furnace to get a loss-on-ignition (LOI) value. Major oxide concentrations were measured from glass discs fused from 0·5 g of powdered sample and 3·5 g of lithium tetraborate flux at 1000 °C. Trace elements were measured directly from pressed pellets containing 7 g of sample bound with a lithium borate binder.

DOI: 10.1002/esp

Samples for clay mineralogical analysis were not subjected to any furnace or oven heating to preserve the lattice structure of expandable clays. Samples were ground and centrifuged to separate all clay material less than 2 μm for analysis. Slides of the samples were analysed using a Siemens D-500 X-ray diffractometer following both air-drying and ethylene glycolization. Each sample was run in triplicate in both air-dried ethylene glycol solvated states. A packed powder version of each sample was also analysed on the same Siemens XRD for bulk mineralogy (Moore and Reynolds, 1997).

We measured abrasion pH on both the pit and the boring samples using saprolite samples hand-ground and mixed 1:1 with distilled water. The sample and water slurry sat for 20 min before measurement with a glass membrane pH electrode. The calibration of the pH electrode was checked both at the beginning and end of the data collection.

To quantify the morphometric parameters impacting the chemical weathering across the site, we surveyed the hillslope using Trimble real-time kinematic GPS survey equipment at a 1–2 m resolution. We determined geomorphic parameters such as slope and curvature using a 7-m grid size, determined by Heimsath *et al.* (1999, 2005) to be optimal for the field site. Our terrain analyses were done using Surfer 8® software from Golden Software.

Field Location

The field site is a west-facing hillslope near the summit of Mount Vision on Inverness Ridge in Inverness, California (Figure 1a). The site is within the bounds of the Point Reyes National Seashore, 3 km west of the San Andreas Fault at an elevation of approximately 300 m, and receives about 800 mm of rain annually with a mediterranean climate. It was used recently to further quantify how soil production varies with soil thickness, and the processes by which soil is transported off the landscape (Heimsath *et al*., 2005). The granitic lithology and climate at the site make it comparable to other California field sites used for chemical weathering studies (e.g. Riebe *et al*., 2001, 2003a, b; White *et al*., 1996, 2001). Similarity in underlying bedrock also enables more straightforward comparison with other chemical weathering studies on granitic landscapes in other climates, such as Puerto Rico (e.g. White *et al*., 1996, 1998; Schulz and White, 1998, Stonestrom *et al*., 1998) and the southeastern United States (Pavich *et al*., 1989; Cleaves, 1993).

The bedrock at the site is the Point Reyes granodiorite (Curtis *et al*., 1958; Spotts, 1962; Chesterman, 1965), which was emplaced during the Santonian age in the late Cretaceous, 83·9 Ma BP (Curtis *et al*., 1958). This granitic intrusion penetrated sedimentary rocks of early Cretaceous age, creating contact metamorphic features and roof pendants (Galloway, 1977). Subsequent erosion removed much of the sedimentary material mantling Inverness Ridge; hydrothermally altered sedimentary bedrock is exposed in small outcrops at a handful of localities across Point Reyes, none of which is near our field site (Weaver, 1949).

Soil cover mantles the saprolite and bedrock with thicknesses between zero and 120 cm. The soil column is a well-mixed, gravelly inorganic B horizon, typically 30–70 cm thick, beneath a thin organic mat, usually 5–10 cm thick. Soils are poorly horizonated and show extensive evidence of bioturbation, which mixes the soil thoroughly and introduces organic matter from the surface into the mineral soil. The soil–saprolite boundary is directly beneath the B horizon as a transitional zone that is typically no thicker than 10 cm. This transition zone is usually marked by a colour and texture change, from the brown A and B soil horizons to a rusty orange of the saprolite that contains relict bedrock texture. While relict rock structure may be difficult to identify in this transition zone, it becomes clear beneath this transition zone and provides a sharp delineation between the mobile soil layer and the in-place, chemically weathered saprolite. Granitic corestones are present on the ground surface, cropping out in places as tors, and within the soil column. Resistant quartz veins also crop out at several places on the hillslope. We observed disaggregated quartz in the soil column and as talus in hummocks beneath each quartz vein outcrop.

Vegetation at the site is grassland, scrub and trees, which were much more extensive before a 1995 wildfire. Heimsath *et al.* (2005) identified biological agents of physical weathering at Point Reyes. Plants bioturbate the soil and aid in the conversion of saprolite into soil. Major grasses are *Avena* and *Bromus* species. Shrubs present are coyote bush (*Bacharis pilularis*), California sagebrush (*Artemisia californica*), poison oak (*Rhus diversiloba*) and lupine (*Lupinus* spp.). Trees at the site are Bishop pine (*Pinus muricata*) and Douglas fir (*Pseudotsuga menziesii*). Hilltops and ridges near the site are covered with shrubs and grasses with small stands of pines, few over 2 m tall. Both hillsides and hollows contain stands of pine and fir and dense thickets of impenetrable brush. Palynological evidence suggests that Pleistocene climate variations caused no significant fluctuations in hillslope erosion rates or processes, although landslide frequency and sediment storage in valleys may have varied (Rypins *et al*., 1989). This evidence for relatively little variation in erosional processes likely to be dominating the production and transport of soil helped guide previous work in the area (e.g. Dietrich *et al*., 1995; Heimsath *et al*., 1997, 2005).

Fauna at the site are also important agents of physical weathering. Pocket gophers (*Thomomys bottae*) burrow extensively across the landscape. Disused gopher burrows were observed in the soil column through the soil–saprolite

DOI: 10.1002/esp

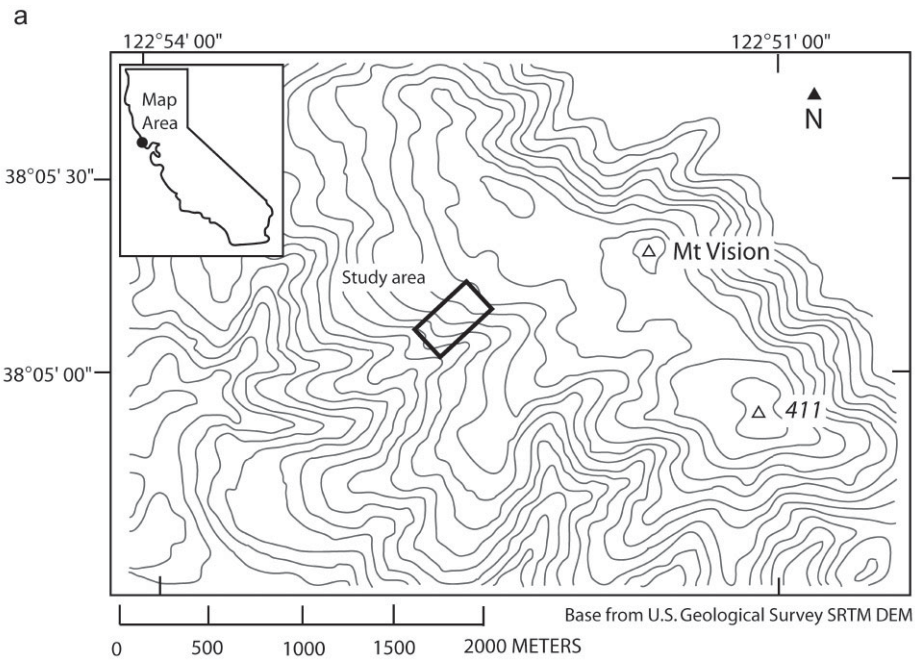

Figure 1. (a) Topographic map of the study region at Point Reyes, California. Contour interval 40 m. Contour lines generated from US Geological Survey Shuttle Radar Topographic Mission data. Black rectangle indicates study area shown in (b). Inset shows site location within California. (b) Location of saprolite pits across field area shown with filled black circles. Numbers above pit locations are soil column thickness (in cm). Contour interval is 1 m. Topography generated from ground-based real-time kinematic GPS survey data and processed to smooth metre-scale variations in the hillslope topography. Figure 1b is shown on the next page.

boundary in several places. Black and Montgomery (1991) and Yoo *et al.* (2005) have shown that pocket gophers are significant transporters of sediment just south of the field area. Other fauna that occupy the site are various species of deer, mountain beavers, small rodents and mountain lion (Evens, 2000). The site and its immediate environs are free from any direct anthropogenic impact with the exception of a disused dirt road cut into the hillslope just downslope of the study area. Soil transport processes have covered most of the road, yielding it nearly invisible. Ranch development in the 1860s in the lowlands of Point Reyes did not extend to the highlands of Inverness Ridge, although small stock ponds dating from the first half of the 20th century are present nearby (Galloway, 1977; Evens, 2000).

Results and Discussion

Chemical and physical weathering

We collected saprolite samples from the base of the soil column in 18 soil pits spanning a divergent nose representative of the field area (Figure 1b). To determine the intensity of chemical weathering and chemical weathering rates, we measured major and trace elements from the pit samples (Table I). Using Zr data from each saprolite sample location (Table II), we calculated chemical weathering rates using Equation 5 and plotted the rates with the soil production rates reported by Heimsath *et al.* (2005) (Figure 2a). These data show for the first time that the chemical weathering rate of saprolite decreases with increasing overlying soil thickness. While the data clearly support an exponential decline of chemical weathering rate with increasing soil thickness ($r^2 = 0{\cdot}78$) they do not reject a linear decline ($r^2 = 0{\cdot}59$). While the physical processes that disrupt and produce soil from the saprolite may result in an exponential decline of soil production rates with increasing soil thickness (Heimsath *et al.*, 1997, 2000), the data from this field site do not reject a linear decline (Heimsath *et al.*, 2005; filled circles in Figure 2a). Given that the chemical processes driving chemical weathering may depend simply on the vertical distance from the ground surface to the soil base, we plot the data on a linear y-axis and acknowledge the potential for an exponential decline. Furthermore, given the variation of soil depths typically observed on upland landscapes, chemical weathering rates vary across the landscape

DOI: 10.1002/esp

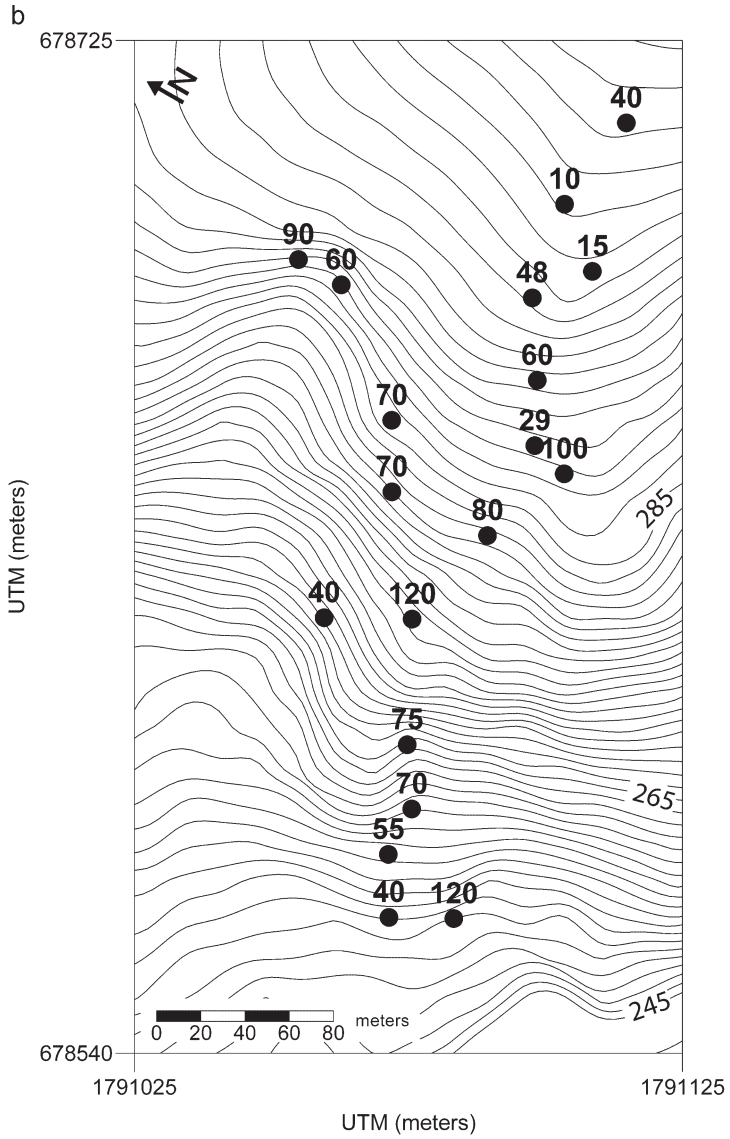

Figure 1. (*Continued*)

in a similar way to the spatial variation of soil production rates. This variation suggests a direct coupling between the physical processes producing soil from the underlying saprolite and the chemical weathering rate of the saprolite.

Chemical weathering intensity measured by abrasion pH does not vary significantly with soil column thickness (Figure 2b). Clay mineralogy data (Table III) indicate, however, that saprolite from beneath thin soil columns is less weathered than saprolite from beneath thick soil columns because non-clay minerals were present only beneath the thinner soils. We attribute the difference between abrasion pH and clay mineralogy to the differences between measuring kinetic properties of the saprolite and qualitative measures of mineralogy within the saprolite. We can establish the magnitude of change between pH data points whereas we cannot distinguish between clay mineralogical samples.

We plot the chemical weathering rates as percentages of total denudation rates against soil column thickness in Figure 2c. Chemical weathering rates from beneath thin soil columns (<60 cm) on divergent sections of the hillslope constitute a large percentage of total denudation. The mean of the six samples is 51 per cent. By contrast, the mean percentage of total weathering of the samples collected from beneath soil columns thicker than 60 cm, and including all samples from the convergent section of the hillslope, is 13 per cent. In comparison, Yoo *et al*. (in press) found that chemical weathering accounted for 40 per cent of total weathering in soils on a hillslope transect on the highlands of

DOI: 10.1002/esp

Table I. Depth, bulk density, and major element compositions of samples and parent from Point Reyes

Pit	Soil column thickness (cm)	Bulk density* ($g\ cm^{-3}$)	SiO_2 (%)	Al_2O_3 (%)	CaO (%)	Na_2O (%)	K_2O (%)	Zr (ppm)
6	15	2·11	75·5	14·9	0·07	0·06	3·01	360
20	15	1·58	44·4	29·0	0·05	0·30	4·21	566
9	29	1·50	61·5	24·4	0·04	0·43	2·41	186
7	40	1·35	90·7	6·1	0·00	0·00	0·60	374
17	40	1·45	65·5	18·8	1·20	2·65	2·67	166
19	40	1·22	65·8	21·0	1·09	1·59	2·59	217
5	48	1·31	66·8	11·7	0·07	0·33	1·44	316
16	55	1·43	60·5	18·1	0·16	1·28	2·72	167
8	60	1·40	64·6	21·3	0·335	0·57	1·64	163
15	70	1·58	53·2	20·9	0·36	0·85	2·71	161
25	70	1·49	67·9	17·9	2·46	1·50	1·93	186
26	70	1·42	65·6	19·3	2·71	2·40	1·68	184
14	75	1·56	54·3	25·4	0·52	1·06	1·79	118
10	80	1·34	52·9	23·0	0·07	0·46	2·29	192
1	90	1·28	58·6	18·3	0·43	0·24	2·08	150
24	100	1·42	66·6	16·5	4·39	3·00	2·37	152
12	120	1·37	62·7	23·3	0·16	0·70	2·51	162
21	120	1·81	65·1	18·7	0·36	1·26	2·25	151
Parent†	–	2·65	59·6	15·5	5·42	2·78	2·74	145

* Bulk density values are means, $n = 3$.

† Parent material concentrations taken from tor sample.

Table II. Chemical weathering rates and intensities at Point Reyes

Pit	Soil column thickness (cm)	Abrasion pH	VR	CIA	PI	SA	CWR-pH ($m\ Ma^{-1}$)	CWR-Zr ($m\ Ma^{-1}$)	SPR* ($m\ Ma^{-1}$)
6	15	4·79	19·9	83	25	5·1	18	35	59
20	15	5·07	6·5	86	41	1·5	16	44	59
9	29	4·79	7·1	89	25	2·5	17	13	58
7	40	4·78	6·1	91	6	14·9	15	31	50
17	40	5·17	3·1	74	42	3·5	13	6	50
19	40	5·36	4·2	80	35	3·1	11	17	50
5	48	4·81	6·8	86	15	5·7	15	27	50
16	55	5·15	5·9	81	32	3·3	9	5	36
8	60	4·85	4·7	89	21	3·0	11	4	36
15	70	5·07	6·7	84	30	2·5	7	2	18
25	70	5·79	2·6	75	32	3·8	5	4	18
26	70	5·41	2·6	74	34	3·4	6	4	18
14	75	5·25	7·2	88	24	2·1	6	1	18
10	80	5·22	9·9	89	23	2·3	4	7	28
1	90	4·76	3·2	87	21	3·2	4	1	14
24	100	5·39	1·7	63	46	4·0	2	1	11
12	120	5·05	7·3	88	21	2·7	3	1	11
21	120	5·38	5·7	83	28	3·5	2	1	11
Parent†	–		1·5	59	48	3·9	0	0	0

* SPR data from Heimsath *et al.* (2005).

† Parent material values calculated from from tor sample concentrations.

southeastern Australia, at the field site used by Heimsath *et al*. (2001). Similarly, Green *et al*. (2006) found that mass losses from soil and saprolite chemical weathering account for between 35 and 55 per cent of total weathering on a different hillslope, at the field site of Heimsath *et al*. (2000) at the base of the Great Escarpment separating the highlands from the coastal lowlands in southeastern Australia.

DOI: 10.1002/esp

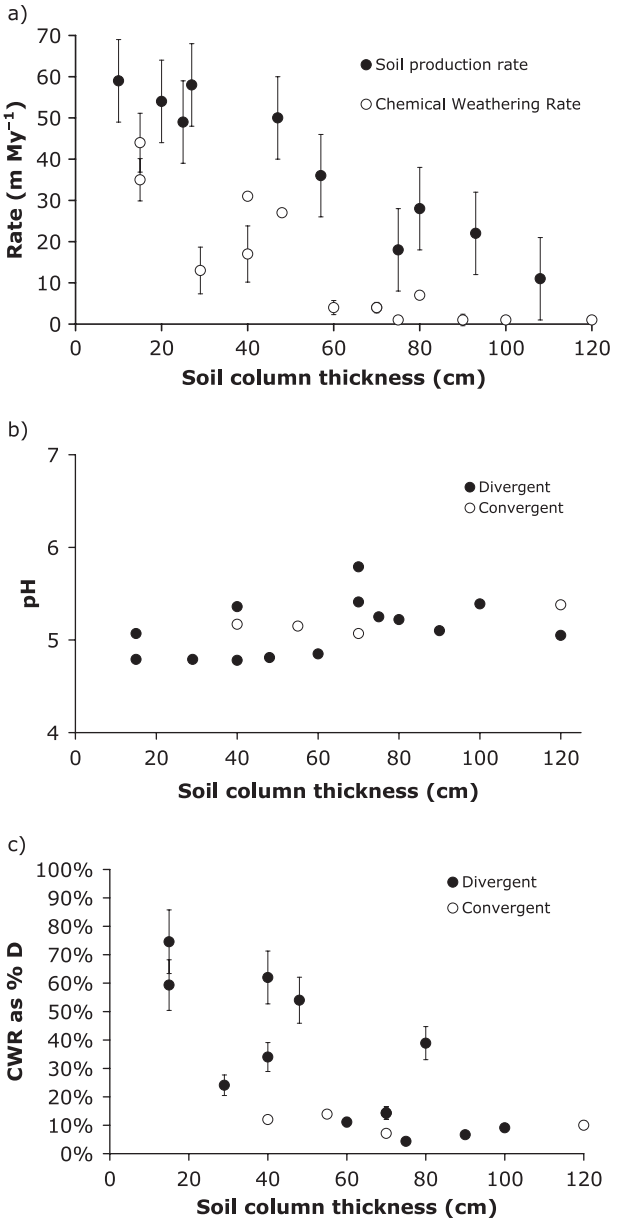

Figure 2. (a) Soil production rate (SPR – filled black circles) and chemical weathering rate (CWR – open circles) (both in m Ma^{-1}) plotted against local soil thickness. CWR calculated from Zr concentrations in the saprolite using Equation 5. Soil production rates were determined using *in situ* produced cosmogenic nuclides ^{10}Be and ^{26}Al, as reported in Heimsath *et al.* (2005). CWR error bars represent all propagated errors of the CWR calculation. (b) Saprolite abrasion pH plotted against soil column thickness (cm). Data from divergent sample locations are shown as filled black circles and the convergent locations are shown as open circles. (c) Chemical weathering rate as a percentage of the landscape denudation rate, *D*, plotted against soil column thickness (cm). Data from divergent sample locations are shown as filled black circles and the convergent locations are shown as open circles. The mean of the six shallowest divergent samples is 51 per cent. The mean of the remaining divergent samples and convergent samples is 13 per cent. Error bars indicate propagated CWR error; some error bars are subsumed by the data points.

Our results comparing chemical and physical weathering rates are thus consistent with previously reported values from other locations. Integral to a discussion of how different weathering processes affect chemical weathering rates and to exploring how hillslope form affects chemical weathering, we examine our data with respect to the topography of the site.

DOI: 10.1002/esp

Table III. Clay minerals data from Point Reyes

Pit	Soil column thickness (cm)	Biotite–vermiculite	Chlorite	Anorthite	Albite
20	15	×	×	×	
9	29	×		×	
7	40	×			
17	40	×	×	×	×
5	48	×			
16	55	×			
8	60	×			
15	70	×			
14	75	×			
10	80	×			
1	90	×			
12	120	×			
21	120	×			
Parent*	–		×	×	×

* Parent material sampled from surface tor.

See Figure 5 for representative traces of deep and shallow pits.

Topographic controls on chemical weathering

We examine our CWR data against the spatial context of the hillslope rather than solely against soil column thickness to examine the role of weathering processes and how they affect rates. First, given that water from both precipitation and subsurface flow is the agent of chemical weathering, topographic controls on hydrology are likely to help explain how chemical weathering varies across the landscape. Studies from other locations, including humid, low-latitude locations like the Rio Icacos catchment (White *et al*., 1996, 1998; Schulz and White, 1998), temperate coastal locations (Anderson *et al*., 2002; Cleaves, 1993), and mountainous, high-elevation sites (Riebe *et al*., 2001; Dethier and Lazarus, 2006) suggest that both precipitation rates and topographic controls on hydrology strongly influence chemical weathering rates and intensities.

Plotting the data from all pit locations, we show that chemical weathering rates decrease with increasing distance from the divide (Figure 3a). Soil column thicknesses also increase in general with distance from the divide (Figure 1b), so a corresponding decrease in chemical weathering rate is not surprising. What is surprising is that chemical weathering intensity also decreases with increasing distance from the divide as shown by the increase in pH of the saprolite samples (Figure 3b). This finding contradicts the suggestion of Figure 2b that chemical weathering intensity does not vary appreciably with soil thickness. This result also contrasts with the results of Green *et al*. (2006), who found that the chemical weathering intensity in saprolite at the soil–saprolite boundary increased with distance from the divide, as soil thickness also increased. With the data presented here, these contradictions cannot be resolved unequivocally. There is some consistency, however counterintuitive it might be, in the suggestion that lower chemical weathering rates are occurring beneath thicker soil depths, which are further from the watershed divide and are less extensively weathered than the saprolite beneath thinner soils.

Saprolite chemical weathering rates shown as percentages of total weathering rates also decrease with distance from the divide (Figure 3c), suggesting that most of the mass loss from the base of the hillslope is likely to be occurring from the soils, particularly from the convergent regions. The soil column is therefore likely to act as an insulator for the saprolite, impeding weathering. In the soils at the base of the passive margin escarpment of southeastern Australia, Green *et al*. (2006) found stratified weathering profiles, suggesting that water infiltration through thick soil columns is incomplete and that less water reaches the saprolite than from under thin soils. Across a similar hillslope, also in southeastern Australia, Yoo *et al*. (in press) found, however, that soil chemical weathering due to sediment transport accounts for increasing mass gain in soils with distance from the divide. We cannot determine whether the mass gains found by Yoo *et al*. (in press) move laterally at a rate too fast for dissolution infiltrating groundwater or whether they dissolve and saturate groundwater such that it achieves kinetic parity with surrounding material. In either case, our data suggest that saprolite beneath thick soil columns is insulated from intense chemical weathering and high rates of weathering.

Examining specifically data from the four pits excavated from the convergent areas at the base of the hillslope, we suggest that the chemical weathering rate increases with increasing contributing surface area (Figure 4a). While these

DOI: 10.1002/esp

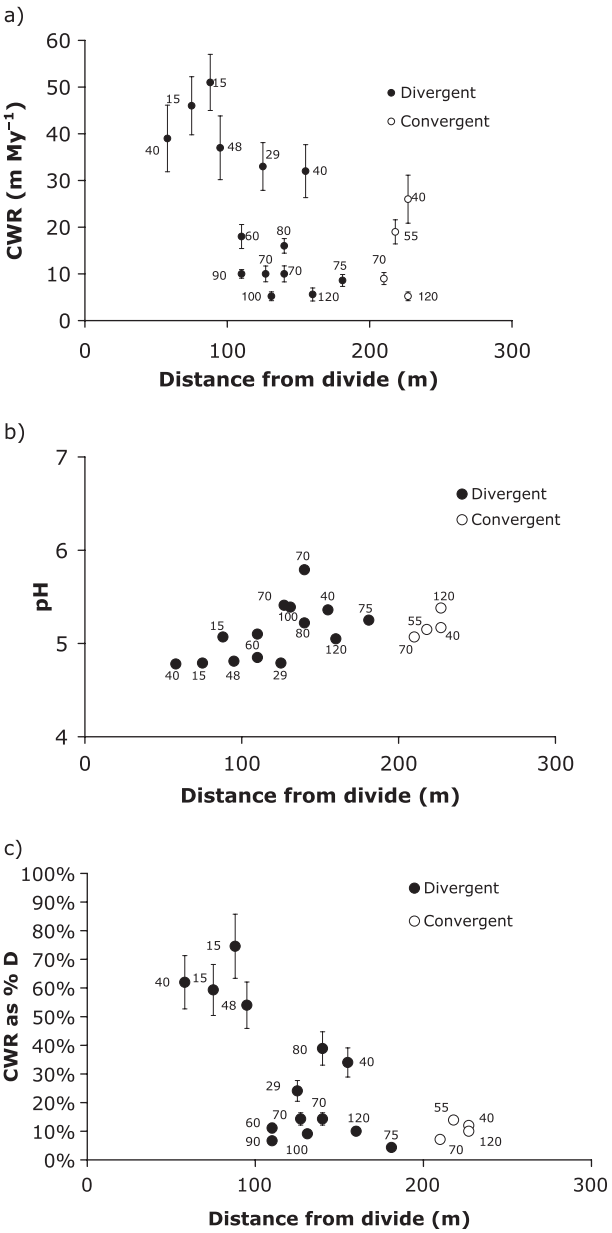

Figure 3. (a) The chemical weathering rate (m Ma^{-1}) plotted against distance from the divide (m). Numbers accompanying each data point indicate the soil column thickness at the sample location. Data from divergent sample locations are shown as filled black circles and the convergent locations are shown as open circles. Error bars indicate 1σ standard error. (b) pH plotted against distance from the divide (m). Numbers next to data points indicate soil column thickness (cm). Data from divergent sample locations are shown as filled black circles and the convergent locations are shown as open circles. (c) Chemical weathering rate as a percentage of the landscape denudation rate, *D*, plotted against soil column thickness (cm). Data from divergent sections of the hillslope are shown as filled black circles. Data from convergent sections of the hillslope are shown as open circles. Error bars indicate propagated CWR error; some error bars are subsumed by the data points.

data are too sparse to make this point more conclusively, the suggestion is compelling. In the context of water availability, weathering rates of the saprolite are likely to increase as more water becomes available for infiltration into the saprolite as upslope contributing surface area increases. The increase in chemical weathering rates also correlates well with a decrease in soil column thickness, potentially driven by overland flow processes becoming active and removing soil from the ground surface. Despite the inference that a larger contributing surface area gathers more

DOI: 10.1002/esp

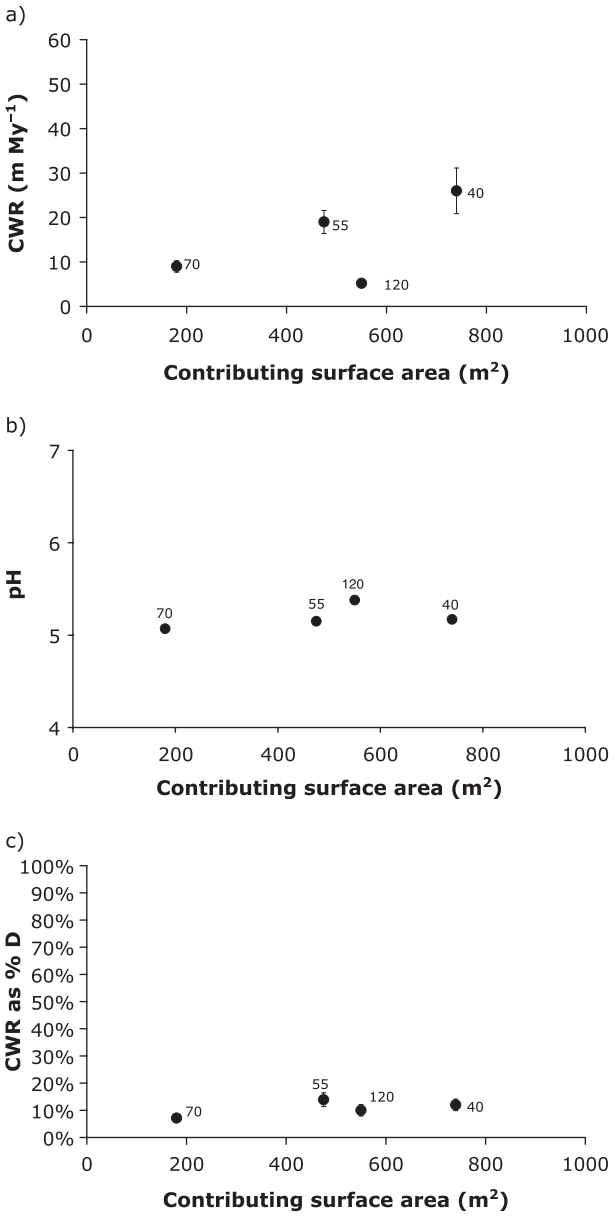

Figure 4. (a) Chemical weathering rate plotted against the upslope contributing surface area (m^2) for sample sites on convergent sections of the hillslope. Numbers next to data points indicate soil column thickness in cm. Error bars represent the propagated error of the soil production rate and Zr measurements. The error bars for the sample labelled '120' are subsumed by the data dot. (b) pH of samples from convergent sites plotted against the upslope contributing surface area (m^2). Numbers next to data points indicate soil column thickness (cm). (c) Chemical weathering rate as a percentage of *D*, the landscape denudation rate, plotted against the upslope contributing area (m^2). Error bars indicate propagated CWR error; some error bars are subsumed by the data points.

water, and evidence from Torres *et al*. (1998) that small precipitation events can lead to large changes in the water retention characteristics of the soil, weathering intensity is even across contributing surface areas (Figure 4b). Chemical weathering rates as a percentage of the total weathering are also roughly even across all contributing surface areas (Figure 4c). While these data may be sparse, they do support reasonable assertions for how topography may control weathering by converging both overland and subsurface flow across the landscape.

DOI: 10.1002/esp

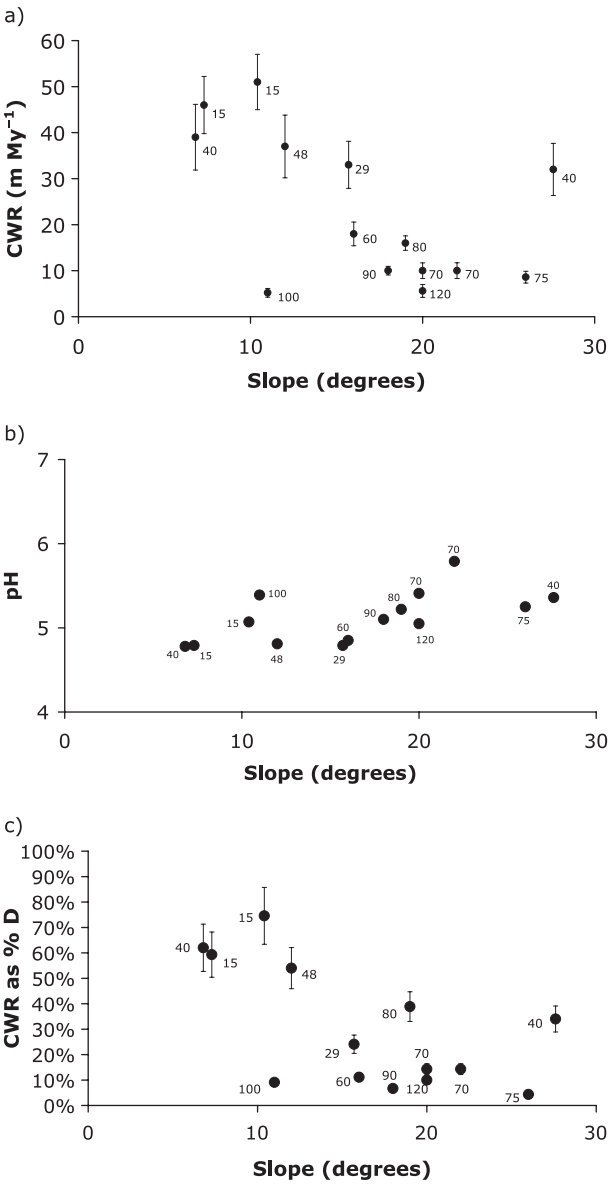

Figure 5. (a) The chemical weathering rate (m Ma^{-1}) plotted against slope (degrees) for divergent samples on the hillslope. Numbers next to data points indicate soil column thickness (cm). Error bars represent the propagated error of the soil production rate and Zr. (b) pH plotted against slope (degrees) for divergent samples on the hillslope. Numbers next to data points indicate soil column thickness (cm). (c) Chemical weathering rate as a percentage of total weathering rate plotted against slope (degrees) for divergent samples on the hillslope. Error bars indicate propagated CWR error; some error bars are subsumed by data points.

Focusing on the samples from divergent regions, where slope-dependent transport processes of soil are thought to be dominant over any potential overland flow processes, we find a decrease in chemical weathering rate with increasing slope (Figure 5a). High chemical weathering rates thus correspond to gentle slopes, while as the slope steepens, the chemical weathering rate decreases and the chemical weathering intensity also decreases as shown by the pH data plotted in Figure 5b. This suggests that steeper slopes promote more precipitation overland flow during storm events, as suggested by Torres *et al*. (1998) and Anderson *et al*. (2002), reducing the potential contact time between water and the saprolite, and that slope angle in addition to soil column thickness act to insulate the saprolite from intense chemical weathering. We now find evidence for overland flow across the field area and therefore suggest that the increasing slope is likely to drive increasing subsurface flow through the soil profile, preventing or minimizing contact

DOI: 10.1002/esp

with the saprolite. Naturally, without extensive subsurface measurements of solute loss and gain (e.g. Anderson *et al*., 2002) this suggestion is not definitive. Nonetheless, plotting saprolite chemical weathering rates as percentages of total weathering rates against slope shows that the contribution of chemical weathering to total denudation decreases with increasing slope (Figure 5c).

As found for divergent ridges on other soil-mantled landscapes (e.g. Heimsath *et al*., 1997, 2000), both soil thickness and slope increase with distance from the divide. Examining weathering from a landscape position perspective, the highest chemical weathering rates, as well as the highest percentage of total denudation, therefore occur under the thin soils near the crest of the hillslope, as well as, to a lesser extent, at the base of the hillslope where contributing area is greatest. This observation naturally begs the question of whether the high chemical weathering rates and high chemical weathering intensities are the result of high rates of precipitation infiltration or whether they are the by-product of the high physical weathering rates under thin soils reported, for example, by Heimsath *et al*. (2005). Since water drives weathering (White *et al*., 1996, 1998; Torres *et al*., 1998; Anderson *et al*., 2002), and high infiltration rates at the top of a hillslope may leave a long-term weathering signature below the saprolite–soil interface, we used samples from the augered bore holes of the saprolite along a transect of the field area to examine chemical weathering at depth in the saprolite.

Figure 6 shows a cross-sectional profile generated from samples collected from the auger holes. Table IV reports the pH values from all of the pit borings. The thickest saprolite profiles on the hillslope, up to 10·9 m, are under the steepest slopes, 20–25°, where the mean soil column is thickest, 70–120 cm. Bedrock is exposed at the top and base of the hillslope where soil column thickness nears zero. Inset plots in Figure 6 show pH data versus depth below ground surface from the auger holes. Every inset within Figure 6 shows lower pH values near the surface and higher pH values at the base of the boring, indicating decreasing weathering with depth, where the greatest depth is either unweathered bedrock, or close to it. In borings from pits 1 and 9, the difference between top and bottom in the pit is nearly 2 pH units, i.e. there is two orders of magnitude difference in H^+ concentration. The water table was not observed in any boring prior to refusal. The symmetric, lens-shaped geometry of the saprolite profile raises questions: why is the thickest saprolite profile under the steepest slopes in the centre of the hillslope and why does the saprolite column pinch out at both the top and bottom of the hillslope? We suggest that the answers to these questions lie within the larger issue of whether there is a geomorphic impact of chemical weathering or whether hillslope form drives chemical weathering signatures.

This problem is ideally suited to a modelling study, which is beyond the scope of this paper. Specifically, modelling the evolution of the landscape with both the soil production and chemical weathering data presented here enables examination of the feedback mechanisms inherent to the problem. For example, in convergent areas of the hillslope, we suggest that chemical weathering rates increase as upslope contributing area increases. This trend over time would lead to increased concavity at the base of the hillslope, thereby increasing the slope in the midslope region at the transition from convex-up to concave-up topography. Increasing concavity over time will lead to thickening soil depths, which will, in turn, drive both soil production and chemical weathering rates down. Similarly, high soil production rates occur under thin soils, which are where slopes are relatively gentle and chemical weathering rates are high, and are found at the top and base of the hillslope. Higher rates over an extended period would increase soil thickness and potentially lead to a feedback to reduce the rates, depending on how the slope evolved. It seems likely, given our observations, that high landscape lowering rates at the top and bottom may be preventing the development of a thick saprolite as observed here (Figure 6). Conversely, the deeper saprolite profile in the midsection of the hillslope may be the result of chemical weathering from infiltrating precipitation from the gently sloped upper portions of the hillslope. To fully reconcile the interplay between physical and chemical processes that results in hillslope evolution, it seems necessary, therefore, to combine data such as those presented here with solute chemistry data (e.g. Anderson *et al*., 2002; White *et al*., 1998) to drive a model (e.g. Mudd and Furbish, 2004). We also point out that almost all soil-mantled landscapes may be susceptible to anthropogenic impact and shallow landsliding or soil slumping. While we did not observe any evidence to suggest that the thinning of soils near the base of the transect is due to either of these impacts, the potential for both remains and must be fully explored when designing similar study areas.

The efficacy of chemical weathering indices

Table II reports pH data as well as chemical weathering intensity index values from all saprolite pits for the Vogt ratio (Vogt, 1927; Kim and Park, 2003), the chemical index of alteration (Kirkwood and Nesbitt, 1991), Parker's index (Parker, 1970), and the silicon–aluminium ratio (Ruxton, 1968). We compare these chemical weathering intensity indices with saprolite abrasion pH measurements to determine the efficacy of each index. Our goal here is to test the robustness of using pH to determine the weathered extent of the saprolite and compare these measurements with indices that have been widely used for similar studies (e.g. Duzgoren-Ayden *et al*., 2002). By verifying our use of

DOI: 10.1002/esp

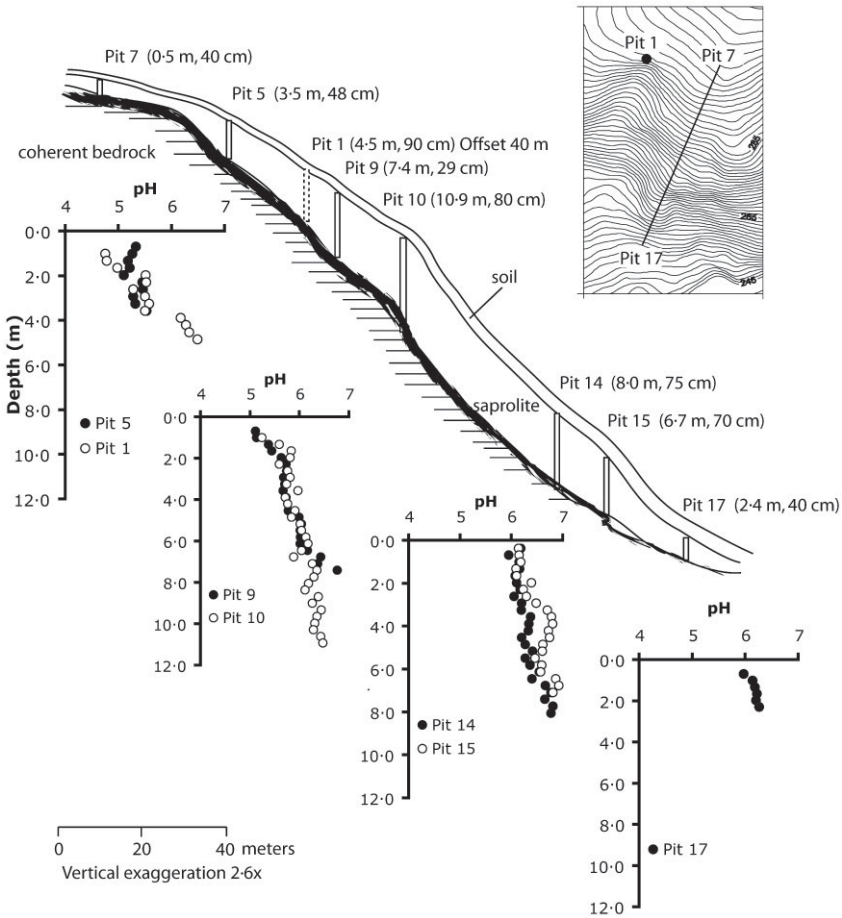

Figure 6. A cross-section schematic showing the thickness of the saprolite column from the top of the hillslope to the bottom. The inset topographic map in the upper right of the figure indicates the location of the cross-section on the study site. Pit labels indicate the pit number with the depth of the boring (in m) and the soil column thickness (in cm) shown in parentheses. The thickness of the soil column is not drawn to scale, but shows roughly the downslope thickening of the soil column and the relative thickness in comparison with the underlying saprolite. The soil–saprolite boundary is the dark line just beneath the ground surface. The coherent bedrock is denoted by horizontal hashing connected to the thickened black line. The saprolite abrasion pH values for samples collected from each of the seven borings are shown in the four inset plots with axes drawn to scale and with the same pH axis units showing increasing weathered extent to the left, toward the y-axis intercept. Unique pit data corresponds to the data symbols shown in the legend of each plot. Pit 1, indicated as a dashed boring, is offset from the cross-section. Vertical exaggeration is 2·6×.

saprolite pH as a measure of the weathered state of the saprolite we therefore support the use of this relatively easy to measure technique. We report the r^2 values for linear trend lines fitted to both the divergent sample set and complete sample set against abrasion pH as a way to evaluate the fitness of these chemical weathering indices (Figure 7). Note again that low pH values indicate a more extensively weathered condition and we plot all our data on axes such that extent of weathering increases to the right.

Voigt ratio (VR). High VR values, indicating a higher intensity of chemical weathering correlate to low pH values, are shown in Figure 7a. Low VR values correspond to pH values between 5 and 6. As pH decreases, VR values increase although there is considerable scatter in the data. We find that this index is less effective than the CIA and PI in capturing the trend in chemical weathering intensity across the hillslope and do not recommend its use.

Chemical index of alteration (CIA). Figure 7b shows the plot of CIA against pH. CIA values between 84 and 90, indicating high intensity weathering, correspond to pH values below 5. CIA values below 75, indicating less intense weathering, correspond to pH values between 5·25 and 6. The assumption that Ca, Na and K decrease as weathering intensity increases and that Al stays mostly immobile (Kirkwood and Nesbitt, 1991) is valid here. This index shows the best correlation with pH as shown by the correlation coefficients noted in the figure caption.

DOI: 10.1002/esp

Table IV. pH values from borings taken downslope at Point Reyes

Depth (m)	Pit 5	Pit 1	Pit 9	Pit 10	Pit 14	Pit 15	Pit 17
0·3					6·16	6·12	
0·6			5·09		5·93	6·13	5·95
1·0	5·71	4·73	5·11	5·22	6·13	6·16	6·12
1·3	5·83	4·76	5·35	5·57	6·14	6·07	6·16
1·6	5·64	4·96	5·42	5·81	6·05	6·08	6·20
1·9	5·68	5·49	5·61	5·79	6·08	6·37	6·18
2·2	5·69	5·50	5·71	5·57	6·15	6·21	6·24
2·6	5·72	5·26	5·72	5·74	6·03	6·27	EOB
2·9	5·63	5·48	5·66	5·79	6·18	6·46	
3·2	5·56	5·56	5·68	5·72	6·17	6·68	
3·5	5·75	5·48	5·65	5·95	6·35	6·76	
3·8	EOB	6·15	5·71	5·69	6·32	6·78	
4·2		6·25	5·74	5·74	6·31	6·70	
4·5		6·31	5·75	5·89	6·18	6·72	
4·8		6·47	5·97	5·82	6·25	6·59	
5·1		EOB	6·02	5·99	6·39	6·58	
5·4			5·99	6·02	6·25	6·44	
5·8			6	6·11	6·34	6·57	
6·1			5·99	6·15	6·52	6·55	
6·4			6·14	6·02	6·38	6·84	
6·7			6·41	5·86	6·64	6·90	
7·0			6·35	6·24	6·75	6·79	
7·4			6·74	6·33	6·63	EOB	
7·7			EOB	6·27	6·79		
8·0				6·16	6·75		
8·3				6·09	EOB		
8·6				6·36			
9·0				6·24			
9·3				6·42			
9·6				6·33			
9·9				6·29			
10·2				6·26			
10·6				6·41			
10·9				6·45			
11·2				EOB			

EOB, End of boring.

Parker's index (PI). Parker's index and pH are plotted in Figure 7c. Low values in the PI, indicating higher intensity weathering, correspond to low pH values. Because this index uses many of the same major elements as the CIA, it is based on many of the same assumptions. We found poor correlation between PI and pH weathering intensity trends.

Silicon–aluminium ratio (SA). The silicon–aluminium ratio correlates with pH as shown in Figure 7d. The index does not include the components of feldspar weathering and does not include the chemical components of secondary minerals, except for Al. Despite that, we found it to have the second best correlation to pH weathering. The assumptions that Si must decrease with increased weathering and that Si loss must correlate with total element loss are generally applicable.

Summary

We find that measuring saprolite pH provides an effective measure of the weathered state of the material from which soil is being produced. pH is easy and inexpensive to measure and is therefore a good way to approximate the weathered condition of soils and saprolite. The relatively good agreement with the widely used CIA supports the use of pH in this study, although coupling pH measurements with measurements of the major and trace oxides will be straightforward for further study on chemical weathering.

DOI: 10.1002/esp

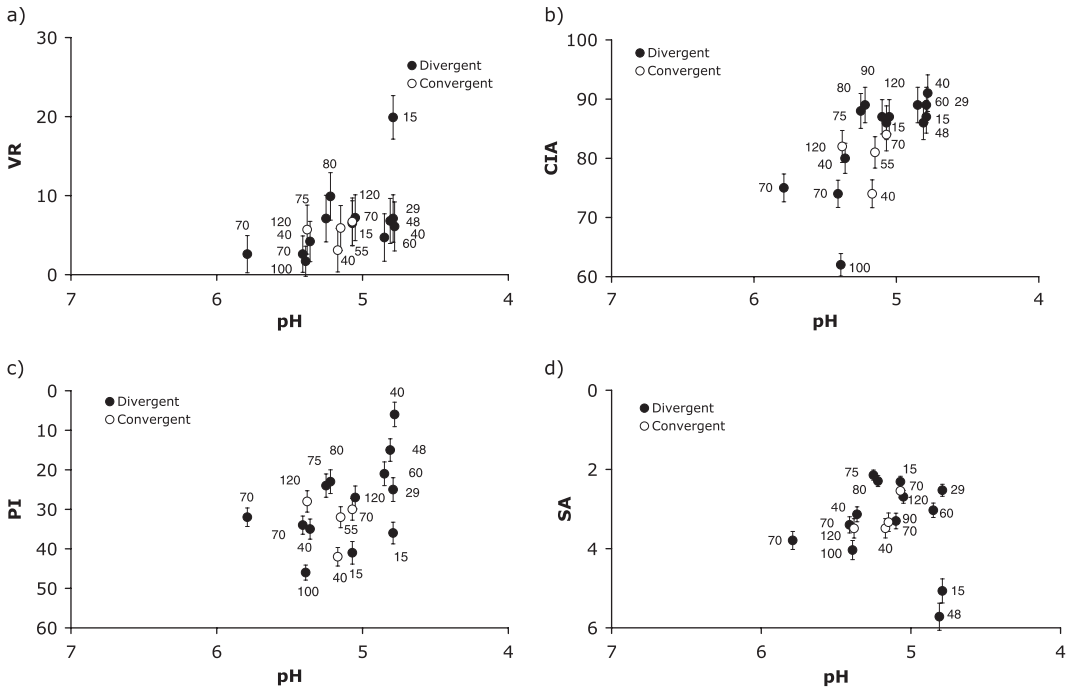

Figure 7. Four chemical weathering indices plotted against saprolite pH. For each index, weathering intensity increases upwards from the base of the y-axis. Weathering as indicated by saprolite pH increases to the right along the x-axis from the intercept with the y-axis (i.e. low pH values indicate higher extent of weathering). Data from divergent sample locations are shown as filled black circles and the convergent locations are shown as open circles. Error bars indicate propagated analytical errors of constituent compounds. Each figure shows the following indices plotted against the saprolite pH: (a) Vogt ratio (VR). Divergent samples $r^2 = 0{\cdot}29$. All samples $r^2 = 0{\cdot}25$. (b) Chemical index of alteration (CIA). Divergent samples $r^2 = 0{\cdot}44$. All samples $r^2 = 0{\cdot}37$. (c) Parker's index (PI). Divergent samples $r^2 = 0{\cdot}32$. All samples $r^2 = 0{\cdot}19$. (d) Silicon–aluminium ratio (SA). Divergent samples $r^2 = 0{\cdot}37$. All samples $r^2 = 0{\cdot}29$.

Conclusions

Our study had two goals: first, to examine the relationship between chemical and physical weathering rates across a landscape; and second, to infer the geomorphic impact of chemical weathering on the same landscape. As part of this study, we also examined the effectiveness of four commonly used indices of chemical weathering intensity to determine which would be most effective in quantifying the chemical weathering variation of granitic saprolite beneath a mobile soil column.

Soil column thicknesses vary across the study area, ranging from zero to 120 cm, while the underlying saprolite contains highly resistant granitic parent minerals and secondary weathering products, mostly biotite–vermiculite clay. Chemical weathering rates decrease with increasing overlying soil thickness, roughly parallel with previously determined soil production rates. We suggest that the physical weathering processes set the chemical weathering rates, which account for between 13 and 51 per cent of total weathering rates and occur in proportions similar to those found in other recent studies of similar soil-mantled upland landscapes, where bioturbation is observed to be the dominant sediment production and transport process. In examining the geomorphic impact of chemical weathering across the hillslope, we find agreement between saprolite abrasion pH, our absolute measure of chemical weathering intensity, and the sample slope and the convergent area contributing surface area of the hillslope. We suggest that because these two geomorphic parameters control the availability of water across divergent and convergent parts of the landscape, respectively, they are effective topographic proxies for the extent and rate of chemical weathering. We find that the upper region of the landscape, which has more gentle slopes, experiences a higher intensity of chemical weathering as well as high chemical weathering rates. Conversely, thicker soils combined with steeper slopes in the middle and lower sections of the hillslope may enable overland or increased subsurface throughflow without allowing for much infiltration of the precipitation to the soil–saprolite boundary. Thicker soils also act as insulation, protecting the saprolite at the soil–saprolite interface from water that does infiltrate.

DOI: 10.1002/esp

Chemical weathering and soil production

The trend between chemical weathering intensity and both slope and contributing surface area suggests that long-term changes in hillslope form are the result of feedback mechanisms between topography, physical weathering and climate. Low chemical weathering rates in the midslope area allow for the development of a thicker saprolite profile. The thickness of the saprolite profile on the midslope would then be a function the landscape lowering rates at the top and bottom of the hillslope and the distance between those two areas. High landscape lowering rates are likely to prevent the development of a thick saprolite horizon. Finally, all four of the chemical weathering intensity indices tested here show at least a weak correlation to the absolute intensity of chemical weathering as shown by saprolite abrasion pH. Nonetheless, the CIA is the only index to show high correlation with the weathering intensity observed by the pH data.

In our examination of data from saprolite across a hillslope at Point Reyes, California, we directly couple rates of soil production and chemical weathering. Furthermore, we find that hillslope morphometry is likely to act to control weathering at a hillslope scale. Further understanding of the spatial variation of chemical weathering at the hillslope scale will be possible through combining field data such as those reported here with a landscape evolution model coupling both physical and chemical weathering processes.

Acknowledgements

We thank Daniel Burke for the XRD analysis of clay samples at the Dartmouth Clay Minerals Lab, Carissa Capuano, Edward Meyer and Gavin Barnard for field assistance, and Dawn Adams at the National Park Service for access to Point Reyes National Seashore. This research was funded by a Geological Society of America Graduate Fellowship grant to B. C. Burke, by a National Science Foundation grant to A. M. Heimsath, and was partially funded under the auspices of the Water Resources Division budget of the US Geological Survey.

References

Ahnert F. 1987. Approaches to dynamic equilibrium in theoretical simulations of slope development. *Earth Surface Processes and Landforms* **12**: 3–15.

Anderson RS, Humphrey NF. 1989. Interaction of weathering and transport processes in the evolution of arid landscapes. In *Quantitative Dynamic Stratigraphy*, Cross T (ed.). Prentice Hall: Englewood Cliffs, NJ; 349–361.

Anderson SP, Dietrich WE, Brimhall GH. 2002. Weathering profiles, mass-balance analysis, and rates of solution loss: linkages between weathering and erosion in a small, steep catchment. *Geological Society of America Bulletin* **114**: 1143–1158.

Banfield JF, Eggleton RA. 1989. Apatite replacement and rare earth mobilization, fractionation, and fixation during weathering. *Clays and Clay Minerals* **37**: 113–127.

Black TA, Montgomery D. 1991. Sediment transport by burrowing mammals, Marin County, California. *Earth Surface Processes and Landforms* **16**: 163–172.

Brimhall GH, Lewis CJ, Ford C, Bratt J, Taylor G, Warin O. 1991. Quantitative geochemical approach to pedogenesis: importance of parent material reduction, volumetric expansion, and eolian influx in laterization. *Geoderma* **51**: 51–91.

Brimhall GH, Chadwick OA, Lewis CJ, Compston W, Willaims IS, Danti KJ, Dietrich WE, Power ME, Hendricks D, Bratt J. 1992. Deformational mass-transport and invasive processes in soil evolution. *Science* **255**: 695–702.

Carson MA, and Kirkby MJ. 1972. *Hillslope Form and Process*. Cambridge University Press: New York.

Chesterman CW. 1965. Descriptive petrography of rocks dredged off the coast of central California. *California Academy of Sciences, Proceedings, 4th Series*, **27**(10): 359–374.

Cleaves ET. 1993. Climatic impact on isovolumetric weathering of a coarse-grained schist in the northern Piedmont Province of the central Atlantic states. *Geomorphology* **8**: 191–198.

Curtis GH, Evernden JF, Lipson J. 1958. *Age determination of some granitic rocks in California by the potassium-argon method*. California Division of Mines Monograph 54.

Dethier DP, Lazarus ED. 2006. Geomorphic inferences from regolith thickness, chemical denudation, and CRN erosion rates near the glacial limit, Boulder Creek catchment and vicinity, Colorado. *Geomorphology* **75**: 384–399.

Dietrich WE, Reiss R, Hsu M-L, Montgomery DR. 1995. A process-based model for colluvial soil depths and shallow landsliding using digital elevation data. *Hydrological Processes* **9**: 383–400.

Duzgoren-Ayden, NS, Ayden, A, Malpas, J. 2002. Reassessment of chemical weathering indices: case study on pyroclastic rocks of Hong Kong. *Engineering Geology* **63**: 99–119.

Evens JG. 2000. *The Natural History of the Point Reyes Peninsula*. Point Reyes National Seashore Association: Olema.

Fernandes NF, Dietrich WE. 1997. Hillslope evolution by diffusive processes: the timescale for equilibrium adjustments. *Water Resources Research* **33**: 1307–1318.

Galloway AJ. 1977. *Geology of the Point Reyes Peninsula, Marin County, California*. Bulletin 202. California Division of Mines and Geology: Sacramento.

Grant WH. 1969. Abrasion pH, an index of chemical weathering. *Clays and Clay Minerals* **17**: 151–155.

DOI: 10.1002/esp

Green EG, Dietrich WE, Banfield JF. 2006. Quantification of chemical weathering rates across an actively eroding hillslope. *Earth and Planetary Science Letters* **242**: 155–169.

Heimsath AM, Dietrich WE, Nishiizumi K, Finkel RC. 1997. The soil production function and landscape equilibrium. *Nature* **388**: 358–361.

Heimsath AM, Dietrich WE, Nishiizumi K, Finkel RC. 1999. Cosmogenic nuclides, topography, and the spatial variation of soil depth. *Geomorphology* **27**: 151–172.

Heimsath AM, Chappell J, Dietrich WE, Nishiizumi K, Finkel RC. 2000. Soil production on a retreating escarpment in southeastern Australia. *Geology* **28**: 787–790.

Heimsath AM, Chappell J, Dietrich WE, Nishiizumi K, Finkel RC. 2001. Late Quaternary erosion in southeastern Australia: a field example using cosmogenic nuclides. *Quaternary International* **83–5**: 169–185.

Heimsath AM, Furbish DJ, Dietrich WE. 2005. The illusion of diffusion: field evidence for depth-dependent sediment transport. *Geology* **33**: 949–952.

Irfan TY. 1996. Mineralogy, fabric properties, and classification of weathered granites in Hong Kong. *Quarterly Journal of Engineering Geology* **29**: 5–35.

Irfan TY. 1999. Characterization of weathered volcanic rocks in Hong Kong. *Quarterly Journal of Engineering Geology* **32**: 317–348.

Jeong GY, Kim HB. 2003. Mineralogy, chemistry, and formation of oxidized biotite in the weathering profile of granitic rocks. *American Mineralogist* **88**: 352–364.

Kim S, Park HD. 2003. The relationship between physical and chemical weathering indices of granites around Seoul, Korea. *Bulletin of Engineering Geology Environment* **62**: 207–212.

Kirkwood DE, Nesbitt HW. 1991. Formation and evolution of soils from an acidified watershed, Plastic Lake, Ontario, Canada. *Geochimica et Cosmochimica Acta* **55**: 1295–1308.

McBride MB. 1994. *Environmental Chemistry of Soils*. Oxford University Press: New York.

Moore DM, Reynolds RF. 1997. *X-Ray diffraction and the Identification and Analysis of Clay Minerals*. Oxford University Press: New York.

Mudd SM, Furbish DJ. 2004. Influence of chemical denudation on hillslope morphology. *Journal of Geophysical Research* **109**: F02001, 1–17.

Murphy SF, Brantley SL, Blum AE, White AF, Dong H. 1998. Chemical weathering in a tropical watershed, Luquillo Mountains, Puerto Rico: II. Rate and mechanism of biotite weathering. *Geochimica et Cosmochimica Acta* **62**: 227–243.

Nesbitt HW, Young GM. 1982. Early Proterozoic climates and plate motions inferred from major element chemistry of lutites. *Nature* **299**: 715–717.

Parker A. 1970. An index of weathering for silicate rocks. *Geological Magazine* **107**: 501–504.

Paton T, Humphries GS, Mitchell PB. 1995. *Soils: A New Global View*. University College Press: London.

Pavich MJ. 1989. *Investigations of the characteristics, origin, and residence time of the Upland residual mantle of the Piedmont of Fairfax County, Virginia*. US Geological Survey Open File Report. US Government Printing Office, Washington, DC.

Riebe CS, Kirchner JW, Granger DE, Finkel, RC. 2001. Strong tectonic and weak climatic control of long-term chemical weathering rates. *Geology* (Boulder) **29**: 511–514.

Riebe CS, Kirchner JW, Finkel RC. 2003a. Long-term rates of chemical weathering and physical erosion from cosmogenic nuclides and geochemical mass balance. *Geochimica et Cosmochimica Acta* **67**: 4411–4427.

Riebe CS, Kirchner JW, Finkel RC. 2003b. Sharp decrease in long-term chemical weathering rates along an altitudinal transect. *Earth and Planetary Science Letters* **67**: 4411–4427.

Roaldset E. 1972. Mineralogy and geochemistry of Quaternary clays in the Numendal area, southern Norway. *Norsk Geologisk Tidsskrift* **52**: 335–369.

Ruxton BP. 1968. Measures of the degree of chemical weathering of rocks. *Journal of Geology* **76**: 518–527.

Rypins S, Reneau SL, Byrne R, Montgomery DR. 1989. Palynologic and geomorphic evidence for environmental change during the Pleistocene-Holocene transition at Point Reyes Peninsular, central coastal California. *Quaternary Research* **32**: 72–87.

Schroeder PA, Melear ND, West LT, Hamilton DA. (in press). Meta-gabbro weathering in the Georgia Piedmont, USA: Implications for global silicate weathering rates. *Chemical Geology*.

Schulz MS, White AF. 1998. Chemical weathering in a tropical watershed, Luquillo Mountains, Puerto Rico; III, Quartz dissolution rates. *Geochimica et Cosmochimica Acta* **63**: 337–350.

Spotts JH. 1962. Zircon and other accessory minerals. Coast Range batholith, California. *Geological Society of America Bulletin* **73**: 1221–1240.

Stallard RF, Edmond JM. 1983. The influence of geology and weathering environmental on the dissolved load. *Journal of Geophysical Research* **88**: 9671–9688.

Stonestrom DA, White AF, Akstin KC. 1998. Determining rates of chemical weathering in soils – solute transport versus profile evolution. *Journal of Hydrology* **209**: 331–345.

Torres R, Dietrich WE, Loague K, Montgomery DR, Anderson SP. 1998. Unsaturated zone processes and the hydrologic response of a steep, unchanneled catchment: *Water Resources Research* **34**: 1865–1879.

Vogt T. 1927. Sulitjelmefeltets geologiog petrografi. *Norsk Geologisk Tidsskrift* **121**: 1–560.

Weaver CE. 1949. *Geology of the Coast Ranges immediately north of the San Francisco Bay region, California*. Memoir 35. Geological Society of America: Boulder.

White AF, Blum AE, Schulz MS, Bullen TD, Harden JW, Peterson ML. 1996. Chemical weathering rates of a soil chronosequence on granitic alluvium; I, Quantification of mineralogical and surface area changes and calculation of primary silicate reaction rates. *Geochimica et Cosmochimica Acta* **60**: 2533–2550.

DOI: 10.1002/esp

White AF, Blum AE, Schulz MS, Vivit DV, Stonestrom DA, Larsen MC, Murphy SF, Eberl D. 1998. Chemical weathering in a tropical watershed, Luquillo Mountains, Puerto Rico; I, Long-term versus short-term weathering fluxes. *Geochimica et Cosmochimica Acta* **62**: 209–226.

White AF, Bullen TD, Vivit DV, Schulz MS, Clow DW. 1999. The role of disseminated calcite in the chemical weathering of granitoid rocks. *Geochimica et Cosmochimica Acta* **63**: 1939–1953.

White AF, Bullen TD, Schulz MS, Blum AE, Huntington TG, Peters NE. 2001. Differential rates of feldspar weathering in granitic regoliths. *Geochimica et Cosmochimica Acta* **65**: 847–869.

Yoo K, Amundsen R, Heimsath AM, Dietrich WE. 2005. Process-based model linking pocket gopher (*Thomomys bottae*) activity to sediment transport and soil thickness. *Geology* **33**: 917–920.

Yoo K, Amundsen R, Heimsath AM, Dietrich WE, Brimhall GH. (in press). Rates of soil chemical weathering and sediment transport on hillslopes: integrating geochemical mass balance with hillslope sediment transport processes. *JGR-Earth Surface*.

DOI: 10.1002/esp